iScience

CellPress
OPEN ACCESS

Article

Galectin-1 induces a tumor-associated macrophage phenotype and upregulates indoleamine 2,3-dioxygenase-1

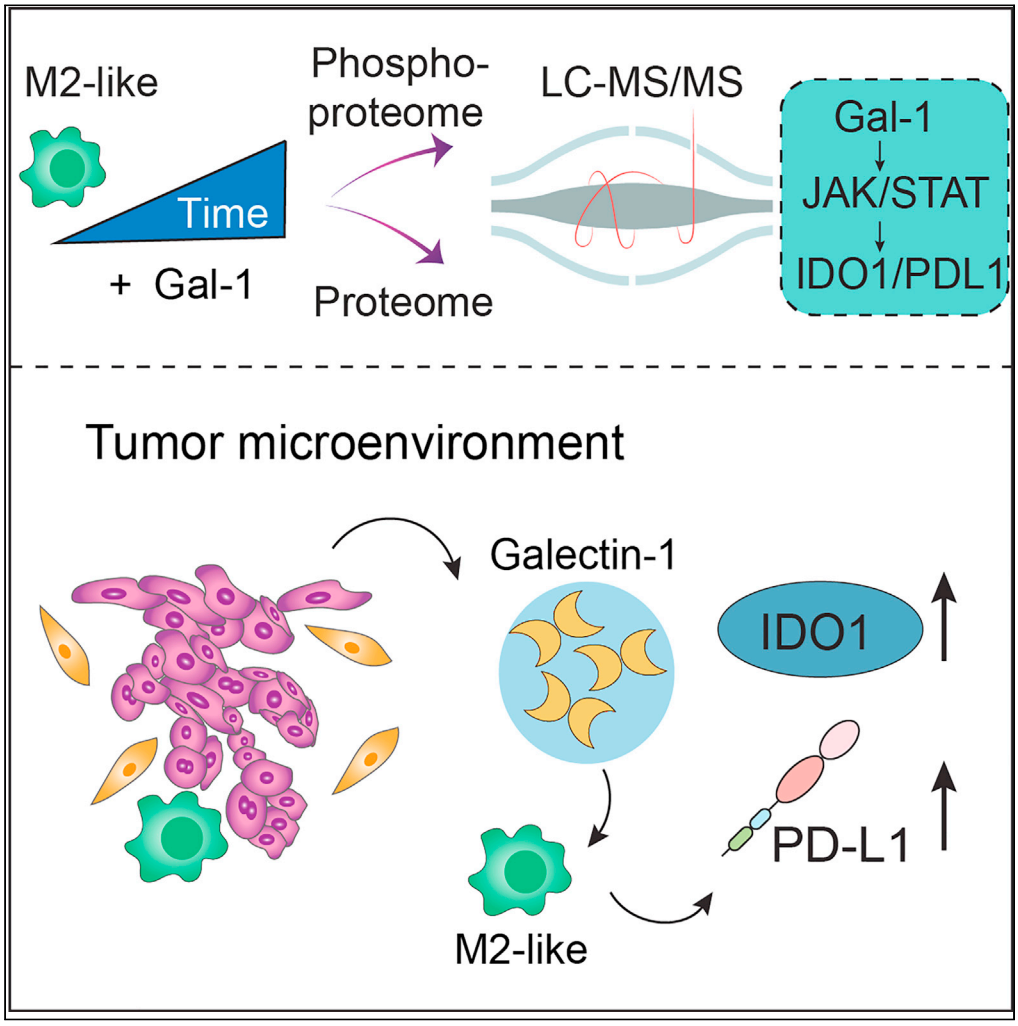

Asha M. Rudjord-Levann, Zilu Ye, Lise Hafkenscheid, ..., Sally Dabelsteen, Jesper V. Olsen, Hans H. Wandall

hhw@sund.ku.dk

Highlights

Gal-1 induces a tumor associated like macrophage phenotype in monocyte-derived MΦs

Gal-1 modulates proteomics landscape of M2-like MΦs

Gal-1 induces expression of IDO1 and PD-L1 in M2-like MΦs but not moDCs

Gal-1 alters the signaling events in M2-like MΦs and activates JAK/STAT signaling

Rudjord-Levann et al., iScience 26, 106984
July 21, 2023
https://doi.org/10.1016/j.isci.2023.106984

iScience

CellPress
OPEN ACCESS

Article

Galectin-1 induces a tumor-associated macrophage phenotype and upregulates indoleamine 2,3-dioxygenase-1

Asha M. Rudjord-Levann,[1,7] Zilu Ye,[1,2,7] Lise Hafkenscheid,[1,7] Sabrina Horn,[1] Renske Wiegertjes,[1] Mathias A.I. Nielsen,[1] Ming Song,[1] Caroline B.K. Mathiesen,[1] Jesse Stoop,[1] Sean Stowell,[3] Per Thor Straten,[4] Hakon Leffler,[5] Sergey Y. Vakhrushev,[1] Sally Dabelsteen,[6] Jesper V. Olsen,[2] and Hans H. Wandall[1,8,*]

SUMMARY

Galectins are a group of carbohydrate-binding proteins with a presumed immunomodulatory role and an elusive function on antigen-presenting cells. Here we analyzed the expression of galectin-1 and found upregulation of galectin-1 in the extracellular matrix across multiple tumors. Performing an in-depth and dynamic proteomic and phosphoproteomic analysis of human macrophages stimulated with galectin-1, we show that galectin-1 induces a tumor-associated macrophage phenotype with increased expression of key immune checkpoint protein programmed cell death 1 ligand 1 (PD-L1/CD274) and immunomodulator indoleamine 2,3-dioxygenase-1 (IDO1). Galectin-1 induced IDO1 and its active metabolite kynurenine in a dose-dependent manner through JAK/STAT signaling. In a 3D organotypic tissue model system equipped with genetically engineered tumorigenic epithelial cells, we analyzed the cellular source of galectin-1 in the extracellular matrix and found that galectin-1 is derived from epithelial and stromal cells. Our results highlight the potential of targeting galectin-1 in immunotherapeutic treatment of human cancers.

INTRODUCTION

Identification of the key immune checkpoints activated in many human cancers has paved the way for successful immunotherapeutic regimens.[1] However, to further develop and improve immunotherapeutic treatment strategies, it is important to continue to decipher how cancer cells antagonize and escape immune-mediated clearance. Galectins are a group of small, secreted, carbohydrate-binding proteins known to play a role during tumorigenesis and as well-known regulators of the immune response.[2–4]

Galectins are characterized by a structurally conserved carbohydrate recognition domain (CRD) with affinity for β-galactosides.[5] Fifteen evolutionarily conserved galectins are found in mammals, 12 of which are found in humans.[6,7] Galectins are structurally classified into prototype galectins, tandem-repeat galectins, and chimera-type galectins.[8] Prototype galectins Gal-1, -2, -5, -7, -10, −11, −13, −14, and −15 comprise one CRD, which can form homodimers, whereas the tandem-repeat galectins Gal-4, -6, -8, -9, and -12 comprise two homologs CRDs that are joined by an amino acid linker.[7] Lastly, the only chimera-type galectin, Gal-3, contains a single CRD fused to an amino acid N-terminal tail.[8] Though all galectins have high affinity toward β-galactose-containing glycoconjugates, such as *N*-acetyllactosamine (LacNAc) and poly-*N*-acetyllactosamine (poly-LacNAc) structures, differences in ligand specificities exist between galectins, conferring functional diversity to individual galectins.[5,9]

Importantly, multivalent oligomerization of galectins at the cell surface results in lattice formation, which is a prerequisite for many biological functions of galectins, enabling galectin-glycan interactions of increased avidity and regulating cell surface receptor stability and endocytosis crucial for tuning cell signaling.[10] Galectins are also known to affect a number of cellular processes through glycan interactions, including cell proliferation, apoptosis, and autophagy.[4,11] This is especially described in relation to the ability of galectins to regulate the immune response. In particular, the regulatory effects of Gal-1 on T cell activation, differentiation, and apoptosis have been well described, resulting in a shift of the overall immune response

[1]Copenhagen Center for Glycomics, Departments of Cellular and Molecular Medicine, Faculty of Health and Medical Sciences, University of Copenhagen, Copenhagen, Denmark

[2]Novo Nordisk Foundation Center for Protein Research, Faculty of Health and Medical Sciences, University of Copenhagen, Copenhagen, Denmark

[3]Department of Pathology, Brigham and Women's Hospital, Boston, MA 02115, USA

[4]Center for Cancer Immune Therapy, Copenhagen University Hospital, Herlev, Denmark

[5]Division of Microbiology, Immunology and Glycobiology, BMC C1228b, Klinikgatan 28, Lund, Sweden

[6]Department of Oral Medicine and Pathology, School of Dentistry, University of Copenhagen, Copenhagen, Denmark

[7]These authors contributed equally

[8]Lead contact

*Correspondence: hhw@sund.ku.dk

https://doi.org/10.1016/j.isci.2023.106984

in favor of a more tolerogenic response.[12,13] However, the ability of Gal-1 to shape the immune system has mostly been ascribed to the effect on T cell compartments. In contrast, the effect of galectins on antigen-presenting cells (APCs) remains more elusive.[14,15]

To address the effect of galectins on APCs, we studied the immune-regulatory effects of Gal-1 on monocyte-derived APCs, including dendritic cells (DCs), M1-like macrophages (MΦs), and M2-like MΦs. Through a combination of transcriptomic, proteomic, and phosphoproteomic analyses, we show that Gal-1 induces differential alterations in APCs, particularly M1-like MΦs and M2-like MΦs. Specifically, Gal-1 induces a tumor-associated macrophage (TAM) phenotype with a combination of pro-inflammatory features and up-regulation of immunomodulators such as checkpoint protein programmed cell death 1 ligand 1 (PD-L1/CD274) and the indoleamine 2,3-dioxygenase-1 (IDO1). Based on our results, we suggest that Gal-1 acts as an early inducer of TAMs in the tumor microenvironment with activation of immune checkpoints including PD-L1/CD274 and IDO1.

RESULTS

Gal-1 is highly expressed in the tumor microenvironment and induces a TAM phenotype profile in monocyte-derived macrophages

First, the expression of Gal-1, Gal-3, and Gal-8 was evaluated in a large set of human tumors compared to normal tissue based on existing databases[16] (Figure 1A). In general, Gal-1 and Gal-3 were significantly upregulated in many of the analyzed tumors, including cholangiocarcinoma, esophageal carcinoma, glioblastoma multiforme, human head and neck squamous cell carcinoma, kidney renal clear cell carcinoma, kidney renal papillary cell carcinoma, lymphoid neoplasm diffuse large B-cell lymphoma, pancreatic adenocarcinoma, sarcoma, skin cutaneous melanoma, stomach adenocarcinoma, and thymoma (Figure 1A). In other tumors, no change or even a decline in Gal-1 expression was observed. This included ovarian cancer, endometrial carcinoma, cervical carcinoma, and lung squamous cell and adenoma carcinomas.[16] No significant difference was seen for Gal-8, except for cholangiocarcinoma. Of note, samples sizes in Figure 1A were variable with a range from 36 to 558 in most cases, except for sarcoma (SARC, n = 2, in normal dataset) and cholangial carcinoma (CHOL, n = 9, in normal dataset) which complicates statistical analysis. Next, we assessed the distribution of Gal-1, Gal-3, and Gal-8 by immunofluorescence in human oral tumors (Figure 1B). For Gal-1, we found increased production in the tumor tissue primarily localized to the tumor stroma (Figure 1B). Gal-3 was also found to be more abundant in the tumors, but, in contrast to Gal-1, Gal-3 was predominantly found in the epithelial tumor cell compartment, with little expression in the tumor stroma (Figure 1B). Subsequently, the expression of Gal-1 was evaluated in the Human Proteome Atlas based on immunolabeling in head and neck cancers, pancreatic adenocarcinomas, gastric adenocarcinomas, and kidney cancers (Figures 1C and S1). Again, we found a similar trend, with stromal accumulation of Gal-1 in most of the evaluated cancers (Figure 1B). The increased expression of Gal-1 was associated with decreased survival in head and neck cancers ($p = 0.0016$) and a non-significant trend of decreased survival in pancreatic cancers ($p = 0.21$) (Figure 1D).

The selective and consistent accumulation of Gal-1 in the tumor stroma prompted us to ask what the function may be on immune cells, which are classically located in the tumor stroma, especially the different APCs, including DCs, and the monocyte-derived macrophages. Therefore, we investigated the transcriptional effects of Gal-1 on different APCs using a well-established model system derived from human peripheral blood mononuclear cells (PBMCs). Three types of APCs were generated: first, the granulocyte-macrophage colony-stimulating factor (GM-CSF)-differentiated M1-like macrophage (MΦ), second, the macrophage colony-stimulating factor (M-CSF)-differentiated M2-like MΦ, and last, the monocyte-derived DCs (moDCs) (Figures 2A and S2A).[17] To assess whether Gal-1 exerts modulatory effects on the genetic profiles of differentiated APCs, we stimulated M1-like MΦs, M2-like MΦs, and DCs with physiological concentrations of Gal-1 (300 ng/mL) for 24 h and performed RNA sequencing compared with non-stimulated cells. A principal-component analysis was performed on the transcripts quantified in all conditions (Figure 2B and Table S1). Without Gal-1 stimulation, M1-like MΦs and M2-like MΦs clustered close together, whereas DCs clustered separately. Comparison of the gene expression profiles before and after Gal-1 stimulation showed that Gal-1 induced a pronounced change in M2-like MΦs and M1-like MΦs. In contrast, Gal-1-stimulated and Gal-1-unstimulated DCs clustered close together, indicating little effect on the transcriptome. Similar results were seen after stimulation with Gal-3, however, to a lesser extent than seen with Gal-1 stimulation (Figures S2B–S2D). Functional enrichment analysis of Gene Ontology (GO) terms revealed that a considerable number of genes were regulated by Gal-1. More specifically, the

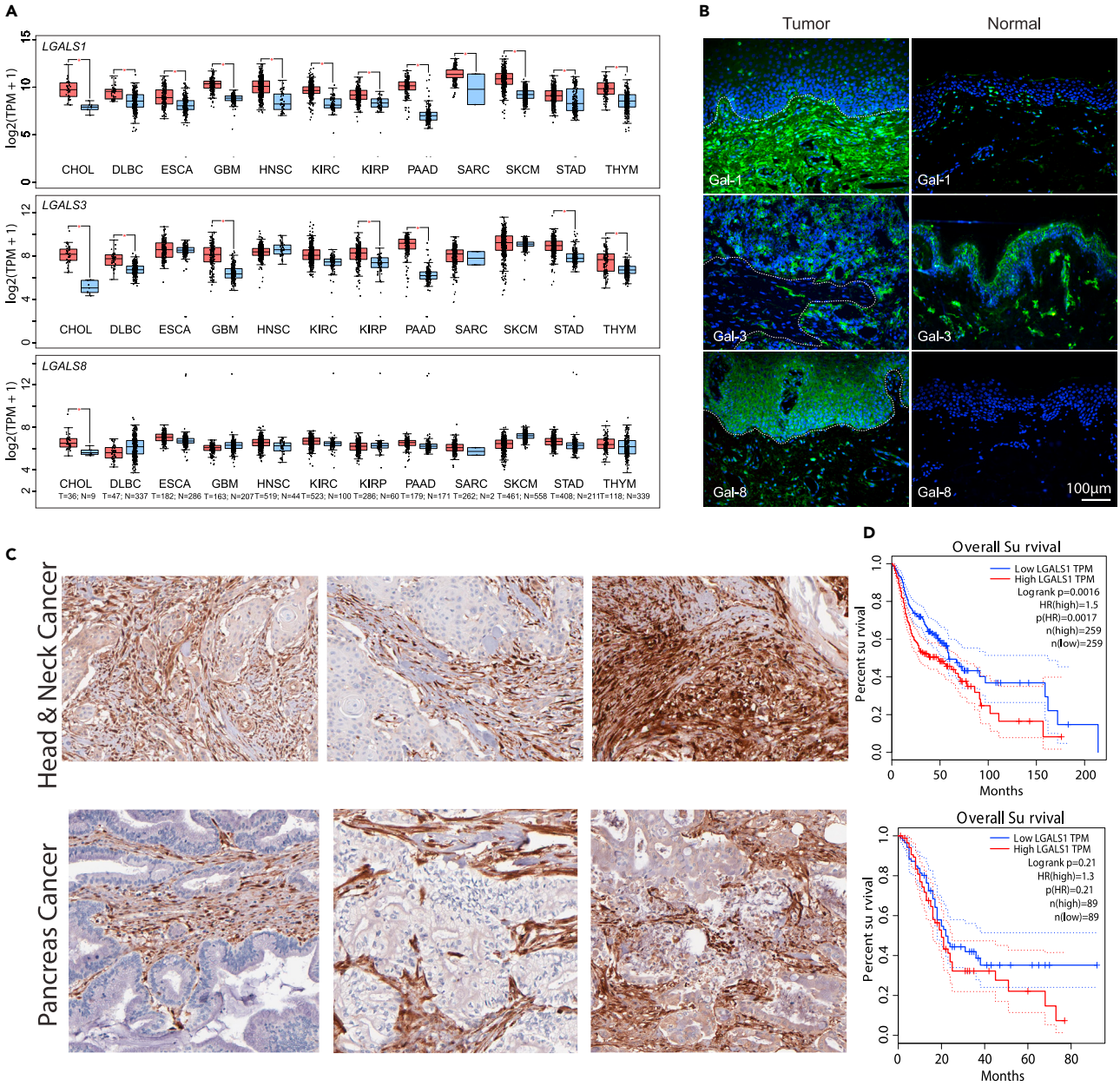

Figure 1. Gal-1 is highly expressed in the tumor microenvironment and associated with decreased survival

(A) RNA sequencing data for LGALS1 (galectin-1), LGALS3 (galectin-3), and LGALS8 (galectin-8) in a number of human tumor samples (red boxes) and the corresponding normal samples (blue boxes).

(B) Immunofluorescent staining of gal-1, gal-3, and gal-8 in oral squamous cell carcinomas and normal human oral epithelia.

(C) Immunohistochemistry of Gal-1 of pancreatic adenocarcinomas and head and neck squamous cell carcinoma. Specimens from three different patients are shown for each cancer. Images were extracted from the Human Proteome Atlas (https://www.proteinatlas.org). In all images Gal-1 is expressed predominantly in the stroma, although expression in the epithelial compartment is also observed in some cancers; a feature that is especially prominent in one of the cases of kidney adenocarcinomas.

(D) Overall survival analysis in head and neck cancer and pancreatic cancer. The survival analysis was done at GEPIA with default settings (http://gepia2.cancer-pku.cn). Data in (A and D) were obtained from the online database GEPIA.[16] CHOL, cholangial carcinoma; DLBC, lymphoid neoplasm diffuse large B-cell lymphoma; ESCA, esophageal carcinoma; GBM, glioblastoma multiforme; HNSC, head and neck squamous cell carcinoma; KIRC, kidney renal clear cell carcinoma; KIRP, kidney renal papillary cell carcinoma; PAAD, pancreatic adenocarcinoma; SARC, sarcoma; SKCM, skin cutaneous melanoma; STAD, stomach adenocarcinoma; THYM, thymoma.

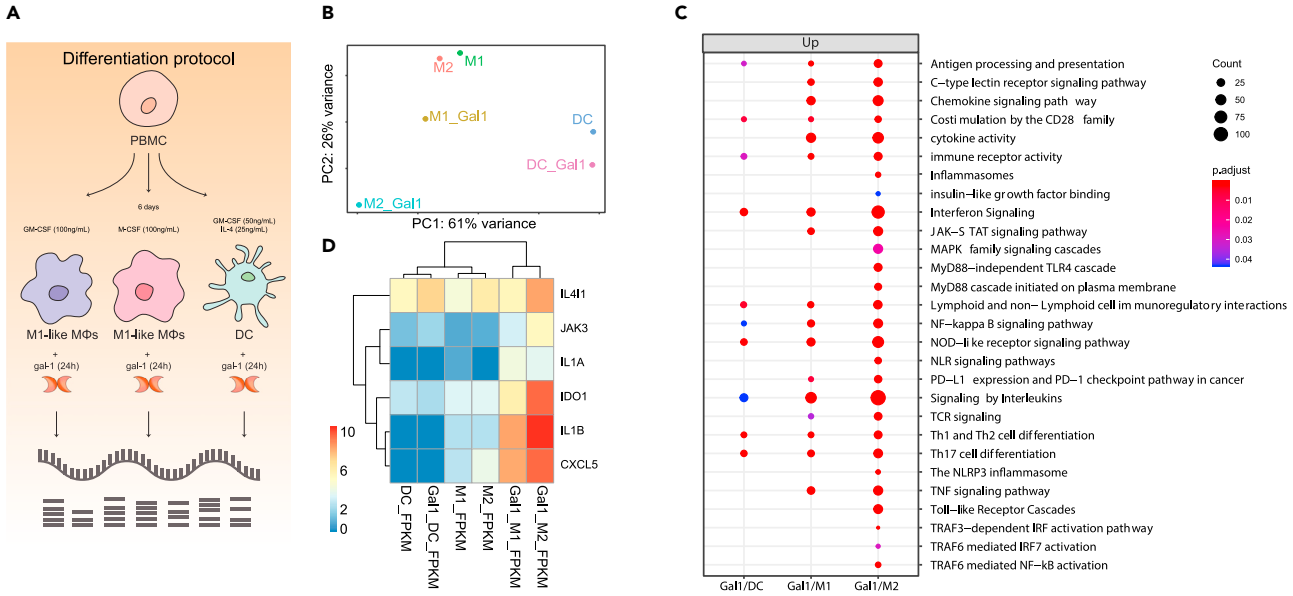

Figure 2. Transcriptional effects of Gal-1 on different antigen-presenting cells

(A) Six-day protocol for isolation and cytokine stimulation of monocytes for differentiation into M1-like MΦs, M2-like MΦs, and DCs. Stimulation with or without Gal-1 (300 ng/mL, 24 h) was performed on day 5 following RNA extraction and processing for RNA sequencing.

(B) Principal-component analysis of transcriptomic data in unstimulated or Gal-1-stimulated M1-like MΦs, M2-like MΦs, and DCs.

(C) Functional enrichment analysis of enriched Gene Ontology terms in Gal-1-stimulated M1-like MΦs, M2-like MΦs, and DCs.

(D) Heatmap of the most regulated genes in M1-like MΦs, M2-like MΦs, and DCs with or without Gal-1.

pathways influenced by Gal-1 involved tyrosine receptor kinase signaling, including interferon (IFN) and JAK/STAT, as well as TLR signaling (Figure 2C and Table S1). In addition, regulated genes were annotated to the modulation of immunoregulatory interactions between lymphoid and non-lymphoid cells, as well as differentiation of lymphoid cells (Figure 2C). Among the upregulated genes assigned to these terms, several key regulators of immune activation were identified, including IDO1, CXCL5, interleukin (IL)-1β, and JAK3 (Figure 2D). We also observed upregulation of IL-4-induced gene 1, which encodes for the immunosuppressive enzyme IL4I1.[18] Most of these pro- and anti-inflammatory components are described to be involved in the tumor microenvironment and tumor-associated MΦ regulation.[19,20] In conclusion, the M2-like MΦs and M1-like MΦs seem to be skewed by Gal-1 toward a phenotype that has been described for TAM regulation.

Gal-1 remodels the proteomic landscape of the M2-like MΦs into a TAM-like phenotype

The pronounced transcriptional effects on M2-like MΦs induced by stimulation with Gal-1, including upregulation of both pro-inflammatory components and key immune regulatory genes consistent with a TAM phenotype, prompted us to focus specifically on the effects of Gal-1 on M2-like MΦs. Therefore, we performed isobaric labeling (tandem mass tag, TMT)-based quantitative proteomic analysis of M2-like MΦs stimulated with or without Gal-1 (300 ng/mL) for 5 min, 6 h, or 12 h on donor 1 (n = 16, 2 replicates for each time point; Figure 3A and Table S2). In addition, the proteomes of M2-like MΦs isolated from three additional donors were analyzed in a label-free manner. In the TMT-based proteome samples, we acquired a comprehensive proteome of M2-like MΦs comprising 8,337 unique proteins with extensive offline high-pH fractionation. Next, we evaluated the fold changes in protein between the different time points of the Gal-1-stimulated samples and controls into soft clustering.[21] This resulted in six clusters, designated clusters 1–6 (Figure 3B). The levels of the M2 lineage markers CD206, CD163, CD11c, and CD14 were comparable over time (Figures S3A and S3B). Upregulated proteins over time, which were clustered in clusters 4 and 6 (Figure 3B), were subjected to functional enrichment analysis based on GO terms. The identified terms were specific to immune system processes (Figure 3C and Table S2) and included regulation of cytokine biosynthesis (tumor necrosis factor [TNF] superfamily, IFN, IL-18), cytokine secretion (IL-1β, IL-1α, IL-18), and cytokine signaling (nuclear factor κB [NF-κB], IFNγ, and IL-2Ra[22]). Interestingly, Gal-1 is also prompted to be involved in the GO terms related to negative regulation of T cell proliferation and activation and increased T cell apoptosis, showing a more tolerogenic and immunosuppressive phenotype

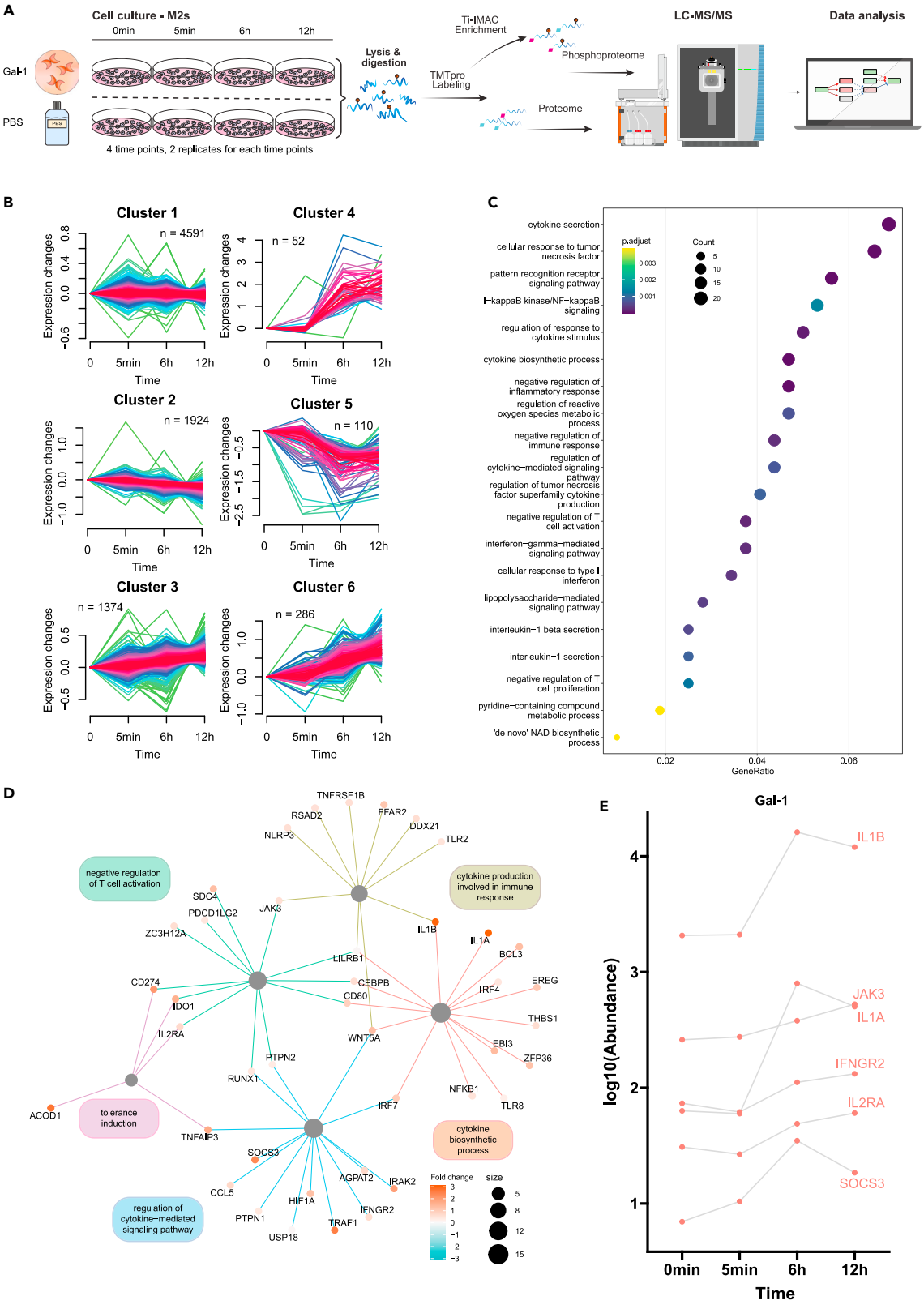
A
Cell culture - M2s
0min
5min
6h
12h
Gal-1
PBS
4 time points, 2 replicates for each time points
Lysis & digestion
Ti-IMAC Enrichment
TMTpro Labeling
Phosphoproteome
Proteome
LC-MS/MS
Data analysis
B
Cluster 1
n = 4591
Cluster 4
n = 52
Cluster 2
n = 1924
Cluster 5
n = 110
Cluster 3
n = 1374
Cluster 6
n = 286
Expression changes
Time
C
cytokine secretion
cellular response to tumor necrosis factor
pattern recognition receptor signaling pathway
I−kappaB kinase/NF−kappaB signaling
regulation of response to cytokine stimulus
cytokine biosynthetic process
negative regulation of inflammatory response
regulation of reactive oxygen species metabolic process
negative regulation of immune response
regulation of cytokine−mediated signaling pathway
regulation of tumor necrosis factor superfamily cytokine production
negative regulation of T cell activation
interferon−gamma−mediated signaling pathway
cellular response to type I interferon
lipopolysaccharide−mediated signaling pathway
interleukin−1 beta secretion
interleukin−1 secretion
negative regulation of T cell proliferation
pyridine−containing compound metabolic process
'de novo' NAD biosynthetic process
p.adjust
Count
GeneRatio
D
negative regulation of T cell activation
cytokine production involved in immune response
tolerance induction
regulation of cytokine−mediated signaling pathway
cytokine biosynthetic process
Fold change
size
E
Gal-1
log10(Abundance)
Time
IL1B
JAK3
IL1A
IFNGR2
IL2RA
SOCS3

Figure 3. Gal-1 modulates the proteomic landscape of M2-like MΦs toward a tumor-associated macrophage phenotype

(A) Overview of the analytical strategy for TMT-based proteomic and phosphoproteomic analysis of M2-like MΦs. M2-like MΦs (n = 16, 1 donor, 2 replicates for each time point) were stimulated with or without Gal-1 (300 ng/mL) for 0 min, 5 min, 6 h, or 12 h. Subsequently, cells were lysed and labeled with TMTpro 16-plex reagents and pooled. A small fraction of pooled sample was reserved for proteome analysis, and the rest was enriched by Ti-IMAC for phosphoproteome analysis. Proteome and phosphoproteome samples were then fractionated and analyzed by LC-MS/MS.

(B) Soft clustering of proteins in Gal-1-stimulated samples. Identified proteins (n = 8337) were clustered into six different clusters based on the ratio distribution across all time points.

(C) Functional enrichment analysis with proteins extracted from clusters 4 and 6.

(D) Network plot of the most regulated proteins and assigned GO terms. The size of the central nodes (gray) indicates the number of proteins represented, and the color of protein nodes indicates log2 fold changes.

(E) Dynamic expression of regulated proteins involved in JAK/STAT signaling in Gal-1-stimulated M2-like MΦs.

(Figure 3C). Among the differentially regulated proteins, a significant upregulation of IFNγ and JAK/STAT signaling components, including JAK3, SOCS3, IL-1β, IL-1α, IL2RA, and IFN gamma receptor 2 (IFNGR2), was found, which was also seen in the transcriptomic data (Figures 3D and 3E).

Moreover, an upregulation of other immunomodulators was observed, including the anti-inflammatory *cis*-aconitate decarboxylase (ACOD1/IRG1), which has been associated with tumor progression (Figure 3E).[23,24] The immune checkpoint protein PD-L1/CD274 was also upregulated in M2-like MΦs after stimulation with Gal-1 and increased over time (6 h and 12 h) compared to unstimulated M2-like MΦs (Figure 3D). Moreover, we conducted a flow cytometry analysis on differentiated monocyte-derived M2-like MΦs and DC after 16 h of 300 ng/mL Gal-1 stimulation, concluding that exposure to Gal-1 upregulates PD-L1 expression (Figure S3C). Lastly, one of the most striking findings was the Gal-1-induced upregulation of IDO1, another key protein in the regulation of immune tolerance (Figure 3D). Our results indicate that Gal-1, among its many effects, exerts immunomodulatory effects on M2-like MΦs, via the expression of IDO1 and upregulation of PD-L1/CD274. Furthermore, IFNγ and IL-1β, IL-1α, and IL2RA are described as immune-reactive tumor microenvironment components and inducers of PD-L1/CD274.[20]

Gal-1 induces expression of IDO1

Because IDO1 was one of the most prominent hits in the global proteome in both TMT-labeled and label-free samples from different donors (Figure 4A and Table S2), the Gal-1-induced expression of IDO1 was confirmed in M2-like MΦs isolated from additional donors by western blot (n = 13 donors) and qPCR (n = 5 donors) (Figures S4A and S4B). Additionally, Gal-1-mediated induction of IDO1 expression was assessed over time, and IDO1 was induced in a dose- and time-dependent manner (Figure 4B). IDO1 is one of two rate-limiting enzymes in L-tryptophan metabolism, in which L-tryptophan is degraded into downstream metabolites, the primary of which is kynurenine. Thus, kynurenine formation serves as a faithful marker of IDO1 activity.[25] As a secondary validation, we evaluated whether the Gal-1-induced expression of IDO1 translates into functional formation of kynurenine in Gal-1-stimulated M2-like MΦs. This was confirmed by kynurenine kinetic assay (Figure 4C). Similar results were seen in Gal-1-stimulated M1-like MΦs but with lower production of kynurenine compared to stimulated M2-like MΦs (Figure S4C). To further determine the kinetics of Gal-1-induced IDO1 activity, kynurenine formation was assessed over time in stimulated M2-like MΦs over 24 h (Figure 4D), demonstrating the formation of kynurenine after 6 h, with increasing production over time (Figure 4D).

Gal-1 alters the signaling events in M2-like MΦs and activates JAK/STAT signaling

To examine the signaling network in M2-like MΦs after Gal-1 stimulation, phosphoproteomic analysis was performed on unstimulated or Gal-1-stimulated M2-like MΦs in the TMT pro-labeled samples (Table S3). We identified 17,283 class I phosphosites, in which the distribution of phosphorylated amino acids was in line with other large-scale phosphoproteomics studies.[26] Similar to the proteome dataset, soft clustering was performed on the phosphosites, which grouped them into six different clusters (Figure 5A). Cluster 4 comprised the most upregulated phosphosites (n = 470). All sites were extracted from this cluster and subjected to functional GO term analysis (Figure 5B and Table S3). Gal-1 stimulation predominantly induced changes in the phosphorylation of proteins that play a role in immune signaling pathways, including NF-κB, Toll-like receptor (TLR), and lipopolysaccharide (LPS), cytokine biosynthesis and metabolism, and myeloid cell differentiation (Figure 5B). The regulated phosphosites were assigned to proteins involved in immune signaling pathways and transcriptional activation, including TRAF6, IRAK4, NF-κB, mitogen-activated protein kinase (MAPK), IL-1β, STAT1, STAT3, and STAT4.

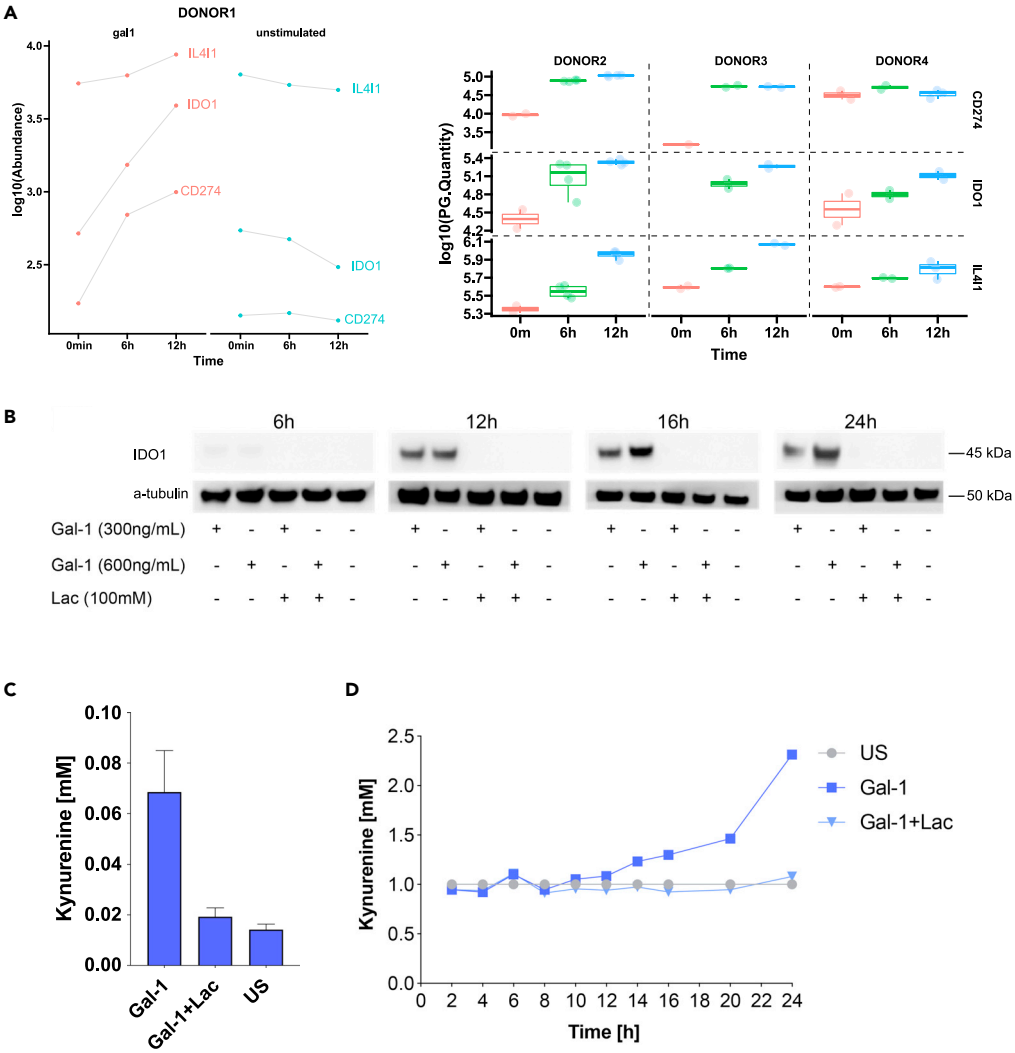

Figure 4. Gal-1 induces expression of IDO1

(A) Dynamic expression of IDO1, PD-L1/CD274, and IL4I1 in Gal-1-stimulated M2-like MΦs. Left: Expression of IDO1 and PD-L1/CD274 in TMT-labeled samples from donor 1. Right: Expression of IDO1, PD-L1/CD274, and IL4I1 in label-free samples from the other three donors.

(B) Expression of IDO1 in M2-like MΦs stimulated with or without Gal-1 (300 ng/mL or 600 ng/mL) and/or lactose (lac) (100 mM) for 6 h, 12 h, 16 h, or 24 h.

(C) Kynurenine formation in M2-like MΦs stimulated with or without Gal-1 (300 ng/mL) and/or lac (100 mM). Data are represented as mean +SEM.

(D) Kynurenine formation over 24 h in M2-like MΦs stimulated with or without Gal-1 (300 ng/mL) and/or lac (100 mM).

Searching for the pathway of IDO1 induction, we found that a high number of regulated tyrosine, serine, and threonine phosphosites in multiple STAT transcription factors were located near a conserved phosphorylation hotspot in proximity to residue 700, which is required for STAT dimerization, nuclear translocation, and transcriptional activation.[27] Among the most prominent sites were the upregulation of serine-733 in STAT4, tyrosine-699 in STAT5B, serine-780 in STAT5A, tyrosine-701 in STAT1, and three sites, serine-727, threonine-714, and tyrosine-705, in STAT3 (Figure 5C). This was further supported by kinase activity analysis, which showed increased activity of JAK2 (Figure S5A). Thus, the identification of STAT phosphosites along with increased JAK2 kinase activity supported the hypothesis that Gal-1 induces IDO1 via activation of the JAK/STAT pathway. Stat3 is activated by phosphorylation at Tyr705, which leads to dimerization, nuclear translocation, and DNA binding. To support the observation that Gal-1 induces JAK/STAT signaling, we performed western blotting using a Phospho-Stat3 (tyrosine-705) monoclonal

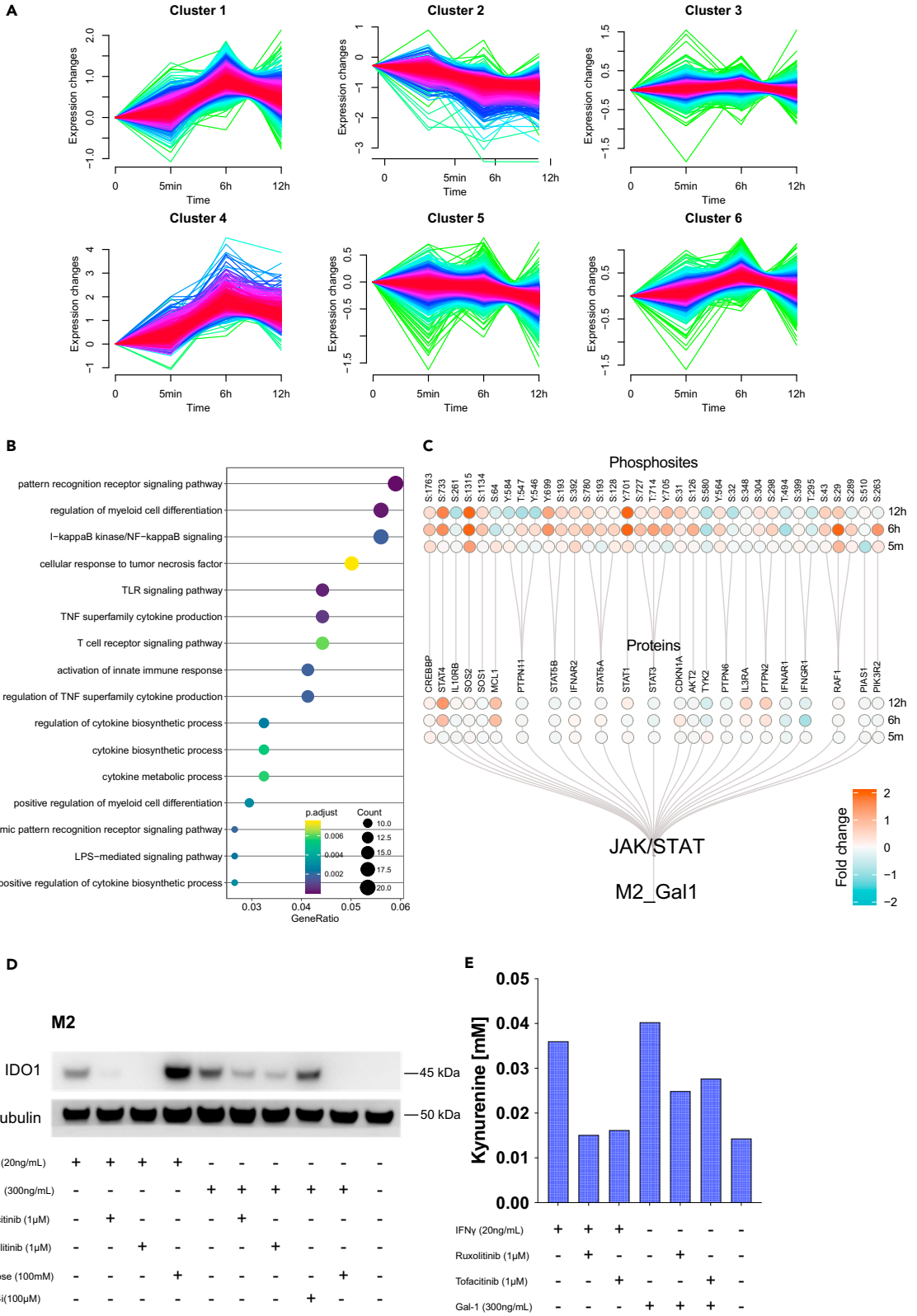
A
Cluster 1
Cluster 2
Cluster 3
Cluster 4
Cluster 5
Cluster 6
Expression changes
Time
0
5min
6h
12h
B
pattern recognition receptor signaling pathway
regulation of myeloid cell differentiation
I−kappaB kinase/NF−kappaB signaling
cellular response to tumor necrosis factor
TLR signaling pathway
TNF superfamily cytokine production
T cell receptor signaling pathway
activation of innate immune response
regulation of TNF superfamily cytokine production
regulation of cytokine biosynthetic process
cytokine biosynthetic process
cytokine metabolic process
positive regulation of myeloid cell differentiation
cytoplasmic pattern recognition receptor signaling pathway
LPS−mediated signaling pathway
positive regulation of cytokine biosynthetic process
p.adjust
Count
GeneRatio
C
Phosphosites
Proteins
12h
6h
5m
JAK/STAT
M2_Gal1
Fold change
D
M2
IDO1
α-tubulin
—45 kDa
—50 kDa
IFNγ (20ng/mL)
Gal-1 (300ng/mL)
Tofacitinib (1μM)
Ruxolitinib (1μM)
Lactose (100mM)
TLR4i(100μM)
E
Kynurenine [mM]
IFNγ (20ng/mL)
Ruxolitinib (1μM)
Tofacitinib (1μM)
Gal-1 (300ng/mL)

Figure 5. Gal-1 alters the signaling events in M2-like MΦs and activates JAK/STAT signaling

(A) Phosphoproteomic analysis of M2-like MΦs stimulated with or without Gal-1 (300 ng/mL) for 0 min, 5 min, 6 h, or 12 h identified 17,283 phosphosites that group into six clusters based on the ratio of distribution over all time points.

(B) Functional enrichment analysis of GO terms assigned to phosphosites in cluster 4.

(C) Map of all phosphosites and assigned proteins in the JAK/STAT signaling pathway with a significant change at any time point. Colors of nodes indicate the log2 fold change in proteins and phosphosites for the different time points.

(D) IDO1 protein expression in M2-like MΦs stimulated with IFNγ (20 ng/mL), Gal-1 (300 ng/mL), JAK/STAT inhibitor tofacitinib (1 μM), ruxolitinib (1 μM), or lactose (100 mM) as indicated for 6 h.

(E) Kynurenine formation in M2-like MΦs stimulated with IFNγ (20 ng/mL), ruxolitinib (1 μM), tofacitinib (1 μM), or Gal-1 (300 ng/mL) as indicated for 6 h.

antibody (mAb), and consistent with our phosphoproteomic data we found activation on tyrosine-705 after Gal-1 stimulation (Figure S5B). To test this hypothesis, unstimulated and Gal-1-stimulated M2-like MΦs were treated with the two JAK/STAT inhibitors ruxolitinib and tofacitinib. Treatment with either inhibitor resulted in decreased expression of IDO1 protein (Figure 5D) and reduced the associated IDO1 activity as indicated by decreased kynurenine formation (Figure 5E). Therefore, Gal-1 acts via the JAK/STAT signaling pathway to induce IDO1 expression in stimulated M2-like MΦs.

Gal-1 is expressed in the tumor microenvironment in response to cross talk between transformed epithelial cells

As shown above, Gal-1 was highly increased in the tumor microenvironment (Figure 1A). This suggests that Gal-1 is either secreted by the tumor cells into the extracellular matrix or deposited by stromal cells in response to signals from the tumor microenvironment. To address these possibilities, we took advantage of our 3D human organotypic tissue models composed of connective tissue with human fibroblasts and overlying stratified epithelia creating a faithful recapitulation of human skin.[28] We have previously shown that the model can be created with genetically engineered keratinocytes[28] and applied to characterize signaling pathways such as transforming growth factor β (TGF-β).[26] Here we used the model to evaluate the expression of Gal-1 in a tumor-like setting using skin tissue models harboring cancer-specific alterations, including knockout (KO) of p53 and overexpression of HRAS. Low expression of Gal-1 was found in both keratinocytes and fibroblasts in wild-type (WT) models (Figure 6A). In contrast, increased Gal-1 expression was measured in both fibroblasts and keratinocytes in models of *HRAS* overexpression or *p53* KO (Figure 6B). These 3D models are devoid of immune cells, indicating that the observed Gal-1 is derived from both the dermal fibroblasts and the tumorigenic keratinocytes. Based on these results, we suggest that cancer cells and cancer-stimulated fibroblasts release Gal-1 that in turn modulates and induces a TAM phenotype with upregulations of IDO1 and PD-L1/CD274 expression via JAK/STAT signaling (Figure 6C).

DISCUSSION

Galectins are well-known immunomodulators, and aberrant expression of galectins frequently occurs in solid tumors.[2,3,29] Though the immunomodulatory effects of galectins are well understood in the context of Gal-1 and its effects on T cells, much less is known about the potential effects of galectin stimulation on APCs. Here, we demonstrated that Gal-1 is upregulated in human epithelial cancers, particularly in the tumor stroma, and promotes the transition of M2-like MΦs and M1-like MΦ toward a TAM-like phenotype. Dynamic proteomic and phosphoproteomic studies showed that Gal-1 induces upregulation of PD-L1/CD274 and IDO1 through JAK/STAT signaling in M2-like MΦs, an effect that was inhibited by the two JAK/STAT inhibitors ruxolitinib and tofacitinib.

Gal-1 is expressed in immune-privileged organs, such as placenta and testis, where it functions to generate a central state of tolerance to prevent autoimmune reactions.[30,31] Gal-1 also promotes the induction of tolerance in tumors, contributing to tumor-immune privilege and evasion of immune surveillance, supporting tumor development and progression.[29,32] The immune-inhibitory effects of Gal-1 have previously been explained primarily by the modulation of T cells.[12,13] Our findings add to this picture by demonstrating that Gal-1 stimulates M2-like macrophages, and to a lesser extent also the M1-like MΦ, to acquire a more tumor-promoting profile similar to TAMs[22] by modulating the transcriptome, proteome, and the signaling landscape of M2-like MΦs.[33–35]

The observed effect of Gal-1 was selective to monocyte-derived macrophages compared to moDCs (Figure 2C). To explain this selectivity, *N*-glycoprofiling of M1-like MΦs, M2-like MΦs, and moDCs was

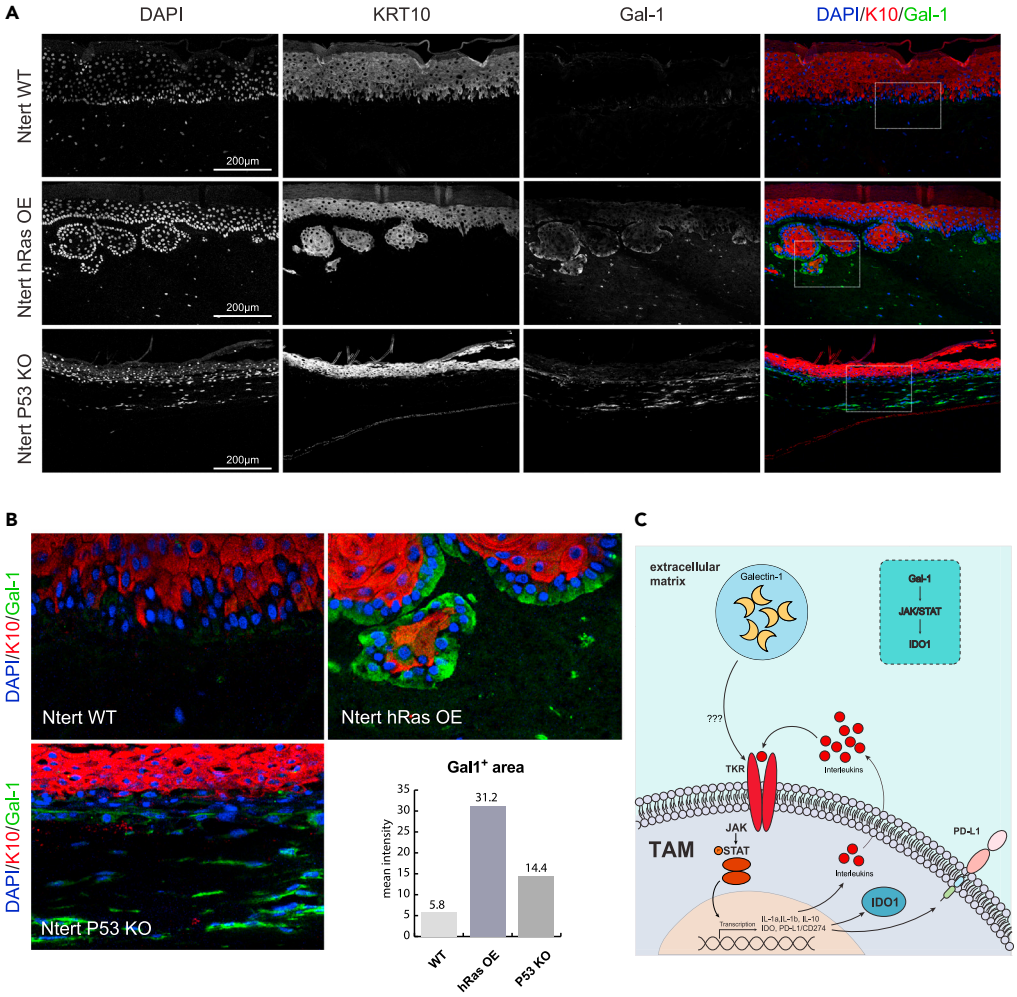

Figure 6. Gal-1 is expressed in the tumor microenvironment in response to cross talk between transformed epithelial cells

(A) Immunofluorescent staining of Gal-1/K10 in WT, hRAS-overexpressing (OE), and P53 KO organotypic models. Gal-1 (green), keratin-10 (K10) (red), and DAPI (blue).

(B) Enlargement of images indicated by white boxes and fold change in the Gal-1^{+} tissue area. Data are presented as mean intensities of the triplicates.

(C) Graphic depiction of the proposed model for the Gal-1-JAK/STAT-IDO1 axis inducing the transition of M2-like MΦs and M1-like MΦ toward TAM-like phenotype. Increased levels of Gal-1 lead to activation of JAK/STAT signaling through yet-unidentified receptor binding/activation. In turn, this induces expression of IDO1, PD-L1/CD274, and a number of cytokines (IL-1α, IL-1β, IL-8, IL-10) acting in a feedback loop to enhance pro-tumorigenic induction of tolerance in M2-like MΦs.

performed by MALDI-TOF-MS (Figure S6). However, this analysis did not reveal any apparent differences in *N*-glycosylation among M1-like MΦs, M2-like MΦs, and moDCs, suggesting that the more predominant effect on M2-like MΦs is more likely caused by inherent differences in receptor profiles and signaling pathways rather than differences in global glycosylation. Notably, it cannot be excluded that the effect is due to changes in branched and elongated *O*-glycans and glycosphingolipids,[36] and it would be helpful to include analyses of this type of glycans in future glycoprofiling experiments.

The Gal-1-induced stimulation of IDO1 secretion from M2-like MΦs was demonstrated at the protein level, both by dynamic proteomics, in western blot analysis, and by functional evaluation of Gal-1-induced enzymatic activity of IDO1 with formation of the primary metabolite kynurenine (Figure 4). Looking for key mediators of IDO1 induction, IFNγ is considered the primary inducer of IDO1 expression and has

been shown to induce IDO1 expression in PBMCs.[37–39] IFNγ-induced activation of the dimeric IFNGR1 and IFNGR2 is known to initiate a signaling cascade via JAK/STAT1 and activation of STAT transcription factors, which can induce IDO1 activation.[40–44] Therefore, we hypothesized that Gal-1 induction of IDO1 occurred via IFNγ signaling and searched for IFNγ-regulated phosphosites in our phosphoproteome (Figure 4). The data revealed an upregulation of several STAT1 phosphosites known to be induced by IFNγ in Gal-1-stimulated M2-like MΦs (Figure 5). Consistent with the involvement of STAT signaling in IDO1 induction, IDO1 expression was inhibited by the two JAK/STAT inhibitors ruxolitinib and tofacitinib (Figure 5). In addition to a direct effect on IFNGR activation, Gal-1 may also potentiate IL receptors, either directly or indirectly, contributing to macrophage activation. This is also suggested by the upregulation of phosphosites in several STAT transcription factors in M2-like MΦs upon Gal-1 stimulation.[45] In addition, Gal-1 stimulation of M2-like MΦs is associated with GO terms for the secretion of several cytokines and chemokines, including IL-1α, IL-1β, CCL5, CXCL8, and IL-18. Furthermore, we identified the induction of GO terms related to the production of IL-1 and IL-18 (Figure 2). These cytokines are known to be highly expressed in the tumor microenvironment, to promote tumor progression, and to be associated with poor overall survival.[46,47] However, it is difficult to determine which of the cytokines are directly or indirectly affected by Gal-1. For example, Gal-1 strongly induces IL-1α expression, which itself promotes the expression of IL-8.[48] Although speculative, this suggests an autocrine mechanism that sustains cytokine-driven JAK/STAT signaling in response to the increased Gal-1 concentration. In conclusion, the activation of JAK/STAT signaling with induction of IDO1, and other tolerogenic proteins, is likely derived from altered IFNγ signaling and locally produced cytokines functioning in an autocrine manner, though this remains to be confirmed in future studies.

In addition to upregulation of IDO1, we also found upregulation of the gene encoding IL4I1 in Gal-1-stimulated M2-like MΦs. IL4I1 belongs to the family of L-amino acid oxidases and is highly expressed in TAMs, where it inhibits the activity of cytotoxic T cells to promote tumor escape.[18,49,50] IL4I1 catalyzes oxidation of L-tryptophan, suggesting that IL4I1 can act in a manner similar to IDO1 to deprive tryptophan, leading to enhanced T cell susceptibility and inhibition.[18] Furthermore, IL4I1 promotes an enhanced M2-like phenotype that is associated with STAT3 and STAT6 activation.[18] Finally, we found upregulation of PD-L1/CD274, the ligand for programmed cell death protein 1, which is expressed on T cells. Upon activation, PD-L1/CD274 negatively regulates the activity of cytotoxic T cells.[51,52] Expression of PD-L1/CD274 on macrophages is induced by the activity of several cytokines, including IL-2 and IL-8.[46,53] This further supports our conclusion that Gal-1 induces a TAM-like phenotype and highlights that this may occur in several ways. Importantly, Gal-1 expression is increased across multiple types of cancer (Figure 1A), which is consistent with the association between Gal-1 and increased tumor aggressiveness, metastasis, and poor prognosis.[32]

Taken together, our data suggest that epithelial tumors produce and secrete Gal-1, primarily from non-lymphoid stromal cells, which induces a TAM phenotype. Thus, in addition to the previously described effects on T cells, Gal-1 modulates MΦ to form a constitutively active microenvironment with a mixed pro-inflammatory and tolerogenic phenotype. This is consistent with the increased Gal-1 expression in many epithelial tumors and the association between Gal-1 and increased tumor aggressiveness, metastasis, and poor prognosis.[32] Our results provide yet another piece of evidence to promote therapeutic strategies to block Gal-1 in human cancers.

Limitations of the study

Due to the challenge of studying human tissue macrophages *in situ*, we used blood-derived monocytes to make monocyte-derived DCs, M1-like, and M2-like macrophages. Therefore, it can be difficult to ensure that the observed effect of galectin-1 for the expression of immunomodulating molecules IDO1 and PD-L1 and the development of TAMs is directly translated to human cancer tissue.

STAR★METHODS

Detailed methods are provided in the online version of this paper and include the following:

- KEY RESOURCES TABLE
- RESOURCE AVAILABILITY
  - Lead contact
  - Materials availability
  - Data and code availability

SUPPLEMENTAL INFORMATION

Supplemental information can be found online at https://doi.org/10.1016/j.isci.2023.106984.

ACKNOWLEDGMENTS

This work was supported by the European Commission (GlycoSkin H2020-ERC), European Commission (Imgene H2020), Lundbeck Foundation, The Danish Research Councils (Sapere Aude Research Leader grant to HW), Danish National Research Foundation (DNRF107), The Friis Foundation, The Michelsen Foundation, A.P. Møller og Hustru Chastine Mc-Kinney Møllers Fond til Almene Formaal, Danish Strategic Research Council, Novo Nordisk Foundation (NNF14CC0001 and NNF17SA0027704), and the program of excellence from the University of Copenhagen (CDO2016). HL was supported by a research grant from Galecto Biotech. We are also grateful for excellent technical assistance from Karin Uch Hansen. We acknowledge the Flow Cytometry & Single Cell Core Facility and the Core Facility for Integrated Microscopy, Faculty of Health and Medical Sciences, University of Copenhagen.

AUTHOR CONTRIBUTIONS

AMRL, ZY, LH, CBKM, JVO, and HHW conceived and designed the study; AMRL, ZY, LH, SH, JS, RW, MAIN, MS, JS, SS, PTS, SV, SD, JVO, and HHW contributed with experimental data and interpretations; HL contributed galectin know-how and materials; AMRL, ZY, LH, and HHW wrote the original manuscript; and all authors edited and approved the final version.

DECLARATION OF INTERESTS

Unrelated to the presented work, Hans Wandall owns stock and is a consultant for and co-founder of EbuMab, ApS. and GO-Therapeutics, Inc. HL is shareholder in Galecto Biotech AB, a company that is developing galectin inhibitors

Received: January 4, 2023
Revised: April 18, 2023
Accepted: May 24, 2023
Published: May 27, 2023

REFERENCES

1. Waldman, A.D., Fritz, J.M., and Lenardo, M.J. (2020). A guide to cancer immunotherapy: from T cell basic science to clinical practice. Nat. Rev. Immunol. *20*, 651–668.

2. Liu, F.-T., and Rabinovich, G.A. (2005). Galectins as modulators of tumour progression. Nat. Rev. Cancer *5*, 29–41.

3. Thijssen, V.L., Heusschen, R., Caers, J., and Griffioen, A.W. (2015). Galectin expression in cancer diagnosis and prognosis: a systematic review. Biochim. Biophys. Acta *1855*, 235–247.

4. Johannes, L., Jacob, R., and Leffler, H. (2018). Galectins at a glance. J. Cell Sci. *131*, jcs208884.

5. Leffler, H., Carlsson, S., Hedlund, M., Qian, Y., and Poirier, F. (2002). Introduction to galectins. Glycoconj. J. *19*, 433–440.

6. Rabinovich, G.A. (1999). Galectins: an evolutionarily conserved family of animal lectins with multifunctional properties; a trip from the gene to clinical therapy. Cell Death Differ. *6*, 711–721.

7. Cummings, R., Liu, F., and Vasta, G. (2017). In Galectins. Essentials of Glycobiology, *Chapter 36*, A. Varki, ed. (Cold Spring Harbor Labo Press).

8. Hirabayashi, J., and Kasai, K. (1993). The family of metazoan metal-independent β-galactoside-binding lectins: structure, function and molecular evolution. Glycobiology *3*, 297–304.

9. Nielsen, M.I., Stegmayr, J., Grant, O.C., Yang, Z., Nilsson, U.J., Boos, I., Carlsson, M.C., Woods, R.J., Unverzagt, C., Leffler, H., and Wandall, H.H. (2018). Galectin binding to cells and glycoproteins with genetically modified glycosylation reveals galectin–glycan specificities in a natural context. J. Biol. Chem. *293*, 20249–20262.

10. Rabinovich, G.A., Toscano, M.A., Jackson, S.S., and Vasta, G.R. (2007). Functions of cell surface galectin-glycoprotein lattices. Curr. Opin. Struct. Biol. *17*, 513–520.

11. Perillo, N.L., Marcus, M.E., and Baum, L.G. (1998). Galectins: versatile modulators of cell adhesion, cell proliferation, and cell death. J. Mol. Med. *76*, 402–412.

12. Rabinovich, G.A., Baum, L.G., Tinari, N., Paganelli, R., Natoli, C., Liu, F.-T., and Iacobelli, S. (2002). Galectins and their ligands: amplifiers, silencers or tuners of the inflammatory response? Trends Immunol. *23*, 313–320.

13. Rabinovich, G.A., and Toscano, M.A. (2009). Turning'sweet'on immunity: galectin–glycan interactions in immune tolerance and inflammation. Nat. Rev. Immunol. *9*, 338–352.

14. Yang, R.-Y., Rabinovich, G.A., and Liu, F.-T. (2008). Galectins: structure, function and therapeutic potential. Expert Rev. Mol. Med. *10*, e17.

15. Ilarregui, J.M., Bianco, G.A., Toscano, M.A., and Rabinovich, G.A. (2005). The coming of age of galectins as immunomodulatory agents: impact of these carbohydrate binding proteins in T cell physiology and chronic inflammatory disorders. Ann. Rheum. Dis. *64*, iv96–iv103.

16. Tang, Z., Li, C., Kang, B., Gao, G., Li, C., and Zhang, Z. (2017). GEPIA: a web server for cancer and normal gene expression profiling and interactive analyses. Nucleic Acids Res. *45*, W98–W102.

17. Mathiesen, C.B.K., Carlsson, M.C., Brand, S., Möller, S.R., Idorn, M., thor Straten, P., Pedersen, A.E., Dabelsteen, S., Halim, A., Würtzen, P.A., et al. (2018). Genetically engineered cell factories produce glycoengineered vaccines that target antigen-presenting cells and reduce antigen-specific T-cell reactivity. J. Allergy Clin. Immunol. *142*, 1983–1987.

18. Yue, Y., Huang, W., Liang, J., Guo, J., Ji, J., Yao, Y., Zheng, M., Cai, Z., Lu, L., and Wang, J. (2015). IL4I1 is a novel regulator of M2 macrophage polarization that can inhibit T cell activation via L-tryptophan and arginine depletion and IL-10 production. PLoS One *10*, e0142979.

19. Cheng, K., Cai, N., Zhu, J., Yang, X., Liang, H., and Zhang, W. (2022). Tumor-associated macrophages in liver cancer: from mechanisms to therapy. Cancer Commun. *42*, 1112–1140.

20. Chen, S., Crabill, G.A., Pritchard, T.S., McMiller, T.L., Wei, P., Pardoll, D.M., Pan, F., and Topalian, S.L. (2019). Mechanisms regulating PD-L1 expression on tumor and immune cells. J. Immunother. Cancer *7*, 305. https://doi.org/10.1186/s40425-019-0770-2.

21. Kumar, L., and E Futschik, M. (2007). Mfuzz: a software package for soft clustering of microarray data. Bioinformation *2*, 5–7.

22. VanDyke, D., Iglesias, M., Tomala, J., Young, A., Smith, J., Perry, J.A., Gebara, E., Cross, A.R., Cheung, L.S., Dykema, A.G., et al. (2022). Engineered human cytokine/antibody fusion proteins expand regulatory T cells and confer autoimmune disease protection. Cell Rep. *41*, 111478. https://doi.org/10.1016/j.celrep.2022.111478.

23. Wu, R., Chen, F., Wang, N., Tang, D., and Kang, R. (2020). ACOD1 in immunometabolism and disease. Cell. Mol. Immunol. *17*, 822–833.

24. Chen, F., Lukat, P., Iqbal, A.A., Saile, K., Kaever, V., van den Heuvel, J., Blankenfeldt, W., Büssow, K., and Pessler, F. (2019). Crystal structure of cis-aconitate decarboxylase reveals the impact of naturally occurring human mutations on itaconate synthesis. Proc. Natl. Acad. Sci. USA *116*, 20644–20654.

25. Badawy, A.A.B., and Guillemin, G. (2019). The plasma [kynurenine]/[tryptophan] ratio and indoleamine 2, 3-dioxygenase: time for appraisal. Int. J. Tryptophan Res. *12*. 1178646919868978.

26. Ye, Z., Kilic, G., Dabelsteen, S., Marinova, I.N., Thøfner, J.F.B., Song, M., Rudjord-Levann, A.M., Bagdonaite, I., Vakhrushev, S.Y., Brakebusch, C.H., et al. (2022). Characterization of TGF-β signaling in a human organotypic skin model reveals that loss of TGF-βRII induces invasive tissue growth. Sci. Signal. *15*, eabo2206.

27. Rane, S.G., and Reddy, E.P. (2000). Janus kinases: components of multiple signaling pathways. Oncogene *19*, 5662–5679.

28. Dabelsteen, S., Pallesen, E.M.H., Marinova, I.N., Nielsen, M.I., Adamopoulou, M., Rømer, T.B., Levann, A., Andersen, M.M., Ye, Z., Thein, D., et al. (2020). Essential functions of glycans in human epithelia dissected by a CRISPR-Cas9-engineered human organotypic skin model. Dev. Cell *54*, 669–684.e7.

29. Girotti, M.R., Salatino, M., Dalotto-Moreno, T., and Rabinovich, G.A. (2020). Sweetening the hallmarks of cancer: galectins as multifunctional mediators of tumor progression. J. Exp. Med. *217*, e20182041.

30. Hirabayashi, J., and Kasai, K. (1984). Human placenta β-galactoside-binding lectin. Purification and some properties. Biochem. Biophys. Res. Commun. *122*, 938–944.

31. Sotomayor, C.E., and Rabinovich, G.A. (2000). Galectin-1 induces central and peripheral cell death: implications in T-cell physiopathology. Dev. Immunol. *7*, 117–129.

32. Rubinstein, N., Alvarez, M., Zwirner, N.W., Toscano, M.A., Ilarregui, J.M., Bravo, A., Mordoh, J., Fainboim, L., Podhajcer, O.L., and Rabinovich, G.A. (2004). Targeted inhibition of galectin-1 gene expression in tumor cells results in heightened T cell-mediated rejection: a potential mechanism of tumor-immune privilege. Cancer Cell *5*, 241–251.

33. Correa, S.G., Sotomayor, C.E., Aoki, M.P., Maldonado, C.A., and Rabinovich, G.A. (2003). Opposite effects of galectin-1 on alternative metabolic pathways of L-arginine in resident, inflammatory, and activated macrophages. Glycobiology *13*, 119–128.

34. Barrionuevo, P., Beigier-Bompadre, M., Ilarregui, J.M., Toscano, M.A., Bianco, G.A., Isturiz, M.A., and Rabinovich, G.A. (2007). A novel function for galectin-1 at the crossroad of innate and adaptive immunity: galectin-1 regulates monocyte/macrophage physiology through a nonapoptotic ERK-dependent pathway. J. Immunol. *178*, 436–445.

35. Yaseen, H., Butenko, S., Polishuk-Zotkin, I., Schif-Zuck, S., Pérez-Sáez, J.M., Rabinovich, G.A., and Ariel, A. (2020). Galectin-1 facilitates macrophage reprogramming and resolution of inflammation through IFN-β. Front. Pharmacol. *11*, 901.

36. Wandall, H.H., Nielsen, M.A.I., King-Smith, S., de Haan, N., and Bagdonaite, I. (2021). Global functions of O-glycosylation: promises and challenges in O-glycobiology. FEBS J. *288*, 7183–7212.

37. Taylor, M.W., and Feng, G.S. (1991). Relationship between interferon-γ, indoleamine 2, 3-dioxygenase, and tryptophan catabolism. FASEB J. *5*, 2516–2522.

38. Yoshida, R., Imanishi, J., Oku, T., Kishida, T., and Hayaishi, O. (1981). Induction of pulmonary indoleamine 2, 3-dioxygenase by interferon. Proc. Natl. Acad. Sci. USA *78*, 129–132.

39. Rubin, B.Y., Anderson, S.L., Hellermann, G.R., Richardson, N.K., Lunn, R.M., and Valinsky, J.E. (1988). The development of antibody to the interferon-induced indoleamine 2, 3-dioxygenase and the study of the regulation of its synthesis. J. Interferon Res. *8*, 691–702.

40. Owen, K.L., Brockwell, N.K., and Parker, B.S. (2019). JAK-STAT signaling: a double-edged sword of immune regulation and cancer progression. Cancers *11*, 2002.

41. Chon, S.Y., Hassanain, H.H., and Gupta, S.L. (1996). Cooperative role of interferon regulatory factor 1 and p91 (STAT1) response elements in interferon-γ-inducible expression of human indoleamine 2, 3-dioxygenase gene. J. Biol. Chem. *271*, 17247–17252.

42. Robinson, C.M., Shirey, K.A., and Carlin, J.M. (2003). Synergistic transcriptional activation

of indoleamine dioxygenase by IFN-γ and tumor necrosis factor-α. J. Interferon Cytokine Res. *23*, 413–421.

43. Litzenburger, U.M., Opitz, C.A., Sahm, F., Rauschenbach, K.J., Trump, S., Winter, M., Ott, M., Ochs, K., Lutz, C., Liu, X., et al. (2014). Constitutive Ido expression in human cancer is sustained by an autocrine signaling loop involving IL-6, STAT3 and the AHR. Oncotarget *5*, 1038–1051.

44. Gough, D.J., Levy, D.E., Johnstone, R.W., and Clarke, C.J. (2008). IFNγ signaling—does it mean JAK–STAT? Cytokine Growth Factor Rev. *19*, 383–394.

45. Morris, R., Kershaw, N.J., and Babon, J.J. (2018). The molecular details of cytokine signaling via the JAK/STAT pathway. Protein Sci. *27*, 1984–2009.

46. Lin, C., He, H., Liu, H., Li, R., Chen, Y., Qi, Y., Jiang, Q., Chen, L., Zhang, P., Zhang, H., et al. (2019). Tumour-associated macrophages-derived CXCL8 determines immune evasion through autonomous PD-L1 expression in gastric cancer. Gut *68*, 1764–1773.

47. Kaplanov, I., Carmi, Y., Kornetsky, R., Shemesh, A., Shurin, G.V., Shurin, M.R., Dinarello, C.A., Voronov, E., and Apte, R.N. (2019). Blocking IL-1β reverses the immunosuppression in mouse breast cancer and synergizes with anti–PD-1 for tumor abrogation. Proc. Natl. Acad. Sci. USA *116*, 1361–1369.

48. Dinarello, C.A. (2018). Overview of the IL-1 family in innate inflammation and acquired immunity. Immunol. Rev. *281*, 8–27.

49. Lasoudris, F., Cousin, C., Prevost-Blondel, A., Martin-Garcia, N., Abd-Alsamad, I., Ortonne, N., Farcet, J.P., Castellano, F., and Molinier-Frenkel, V. (2011). IL4I1: an inhibitor of the CD8+ antitumor T-cell response in vivo. Eur. J. Immunol. *41*, 1629–1638.

50. Carbonnelle-Puscian, A., Copie-Bergman, C., Baia, M., Martin-Garcia, N., Allory, Y., Haioun, C., Crémades, A., Abd-Alsamad, I., Farcet, J.-P., Gaulard, P., et al. (2009). The novel immunosuppressive enzyme IL4I1 is expressed by neoplastic cells of several B-cell lymphomas and by tumor-associated macrophages. Leukemia *23*, 952–960.

51. Jiang, Y., Li, Y., and Zhu, B. (2015). T-cell exhaustion in the tumor microenvironment. Cell Death Dis. *6*, e1792.

52. Bardhan, K., Anagnostou, T., and Boussiotis, V.A. (2016). The PD1: PD-L1/2 pathway from discovery to clinical implementation. Front. Immunol. *7*, 550.

53. Kinter, A.L., Godbout, E.J., McNally, J.P., Sereti, I., Roby, G.A., O'Shea, M.A., and Fauci, A.S. (2008). The common γ-chain cytokines IL-2, IL-7, IL-15, and IL-21 induce the expression of programmed death-1 and its ligands. J. Immunol. *181*, 6738–6746.

54. Salomonsson, E., Carlsson, M.C., Osla, V., Hendus-Altenburger, R., Kahl-Knutson, B., Oberg, C.T., Sundin, A., Nilsson, R., Nordberg-Karlsson, E., Nilsson, U.J., et al. (2010). Mutational tuning of galectin-3 specificity and biological function. J. Biol. Chem. *285*, 35079–35091. https://doi.org/10.1074/jbc.M109.098160.

55. Dickson, M.A., Hahn, W.C., Ino, Y., Ronfard, V., Wu, J.Y., Weinberg, R.A., Louis, D.N., Li, F.P., and Rheinwald, J.G. (2000). Human keratinocytes that express hTERT and also bypass a p16(INK4a)-enforced mechanism that limits life span become immortal yet retain normal growth and differentiation characteristics. Mol. Cell Biol. *20*, 1436–1447.

56. Degen, M., Natarajan, E., Barron, P., Widlund, H.R., and Rheinwald, J.G. (2012). MAPK/ERK-dependent translation factor hyperactivation and dysregulated laminin γ2 expression in oral dysplasia and squamous cell carcinoma. Am. J. Pathol. *180*, 2462–2478.

57. Marinova, I.N., Wandall, H.H., and Dabelsteen, S. (2021). Protocol for CRISPR-Cas9 modification of glycosylation in 3D organotypic skin models. STAR Protoc. *2*, 100668.

58. Yang, Z., Wang, S., Halim, A., Schulz, M.A., Frodin, M., Rahman, S.H., Vester-Christensen, M.B., Behrens, C., Kristensen, C., Vakhrushev, S.Y., et al. (2015). Engineered CHO cells for production of diverse, homogeneous glycoproteins. Nat. Biotechnol. *33*, 842–844.

STAR★METHODS

KEY RESOURCES TABLE

REAGENT or RESOURCE	SOURCE	IDENTIFIER
Antibodies		
anti-IDO1 clone 1F8.2	Sigma-Aldrich	Cat#MAB10009; RRID:AB_1977068
anti-α-tubulin	Abcam	Cat#ab4074; RRID:AB_2288001
anti-phospho-STAT3 (Y705) antibody	Cell signaling Technologies	Cat#9145; RRID:AB_2491009
anti-GAPDH	Abcam	Cat#ab8245; RRID:AB_2107448
HRP-conjugated mouse-anti rabbit	Dako/Agilent	Cat#P0260; RRID:AB_2636929
anti-galectin-1	Abcam	Cat#ab25138; RRID:AB_2136615
anti-galectin-3	R&D	Cat#MAB11541
anti-galectin-8	Abcam	Cat# ab109519; RRID:AB_10861755
anti-cytokeratin 10 (K10)	Dako (Agilent).	Cat#M7002
goat anti-mouse Alexa Flour 594™	Molecular Probes	Cat# A-11005; RRID:AB_141372
goat anti-rabbit Alexa Flour 488™	Molecular Probes	Cat#A-11008; RRID:AB_143165
goat anti-mouse Alexa Flour 488™.	Molecular Probes	Cat#A-11029; RRID:AB_2534088
Alexa Fluor™ 594 Phalloidin	Thermo Fisher Scientific	Cat#A12381
anti-CD206 clone 15.02	Biolegend	Cat#321104; RRID:AB_57190
CD11c-PE	BD Pharmingen	Cat#555392
anti-CD14-PE clone TÜK4	Dako	Cat#R086401-2
CD163-APC	Biolegend	Cat#333609; RRID:AB_2291272
anti-HLA-DR/DP/DQ-FITC clone CR3/43	BD pharmingen	Cat#555558; RRID:AB_395940
CD80-FITC	ebioscience	Cat#11-0809-73
anti-CD40-APC	Biolegend	Cat# 334310
anti-CD86-PE	BD pharmingen	Cat#555665; RRID:AB_396019
anti-PD-L1	Biolegend	Cat#329708; RRID:AB_940360
Secondary antibody Alexa Fluor 488 goat anti-mouse IgG (H+L)	BD pharmingen	Cat#554001; RRID:AB_395197
mouse IgG2bk-PE	BD pharmingen	Cat#555743; RRID:AB_396086
mouse IgG2bk-APC	BD pharmingen	Cat#555745; RRID:AB_398612
mouse IgG2bk-FITC	BD pharmingen	Cat#555742; RRID:AB_396085
Bacterial and virus strains		
E. coli BL21 Star (DE3) cells	Invitrogen	Cat#C601003
Chemicals, peptides, and recombinant proteins		
Lymphoprep	Stem Cell Technologies	Cat#07851
RPMI 1640 with Glutamax	Gibco	Cat#61870036
heat-inactivated human AB serum	Sigma-Aldrich	Cat#H3667
GM-CSF	Peprotech	Cat#300-03
M-CSF	Peprotech	Cat#300-25
IL-4	Peprotech	Cat#200-04
CD14 magnetic beads	Miltenyi	Cat#130-050-201
lactose	Sigma-Aldrich	Cat#61345
L-Tryptophan	Merck	Cat#T0254-1G
30% trichloroacetic acid	Sigma-Aldrich	Cat#T0699-100mL

(*Continued on next page*)

Continued

REAGENT or RESOURCE	SOURCE	IDENTIFIER
2% Ehrlich reagent (4-(dimethylamino)-benzaldehyde	Sigma Aldrich	Cat#156477
Gal-1	Hakon Leffler Lab, Salomonsson et al.[54]	N/A
Gal-1 C3S mutant	Hakon Leffler Lab, Salomonsson et al.[54]	N/A
Gal-3	Hakon Leffler Lab, Salomonsson et al.[54]	N/A
NHS-fluorescein	Thermo Fisher Scientific	Cat#46410
BCA assay	Thermo Fisher Scientific	Cat#23227
Deposited data		
Mass spectrometry proteomics data	ProteomeXchange Consortium via the PRIDE partner repository	PRIDE: PXD034623
Experimental models: Cell lines		
MRC-5	ATCC	Cat#CCL-171, RRID:CVCL_0440
N/TERT-1	James G. Rheinwald, Harvard Institute of Medicine, Dickson et al.[55]	N/A
N/TERT-1 hRas	James G. Rheinwald, Harvard Institute of Medicine, Degen et al.[56]	N/A
N/TERT-1 p53 KO	This paper	N/A
Software and algorithms		
Spectronaut	Biognosys, Zurich, Switzerland	https://biognosys.com/software/spectronaut
Proteome Discoverer	Thermo Fisher Scientific	RRID:SCR_014477
DAPAR	Bioconductor	https://www.bioconductor.org/packages/release/bioc/html/DAPAR.html
clusterProfiler	Bioconductor	RRID:SCR_016884
Mfuzz	Bioconductor	RRID:SCR_000523
FlowJo	Becton, Dickinson & Company	RRID:SCR_008520
FlowLogic	FlowLogic	RRID:SCR_020942
Zen software	ZEISS Microscopy	RRID: SCR_013672
Graphpad Prism	GraphPad Software	RRID:SCR_002798
R and RStudio	Posit	https://posit.co/download/rstudio-desktop/

RESOURCE AVAILABILITY

Lead contact

Further information and requests for resources and reagents should be directed to and will be fulfilled by the lead contact, Hans H. Wandall (hhw@sund.ku.dk).

Materials availability

This study did not generate new unique reagents. All the cell lines used in this manuscript will be made available upon request. A material transfer agreement will be required prior to sharing of materials.

Data and code availability

- The mass spectrometry proteomics data have been deposited to the ProteomeXchange Consortium via the PRIDE partner repository with the dataset identifier PXD034623.

- All code and any additional information required to reanalyze the data reported in this paper is available from the lead contact upon request.
- The information of patient samples from the Human Proteome Atlas was listed in Table S4.

EXPERIMENTAL MODEL AND STUDY PARTICIPANT DETAILS

Ethics statement human blood donors

Buffy coats were obtained from anonymous healthy blood donors. Written informed consent was obtained from the blood donors at the Department of Clinical Immunology in Copenhagen and used without the possibility of identifying case-specific information. Research use of these buffy coats was approved by the ethical committee of Copenhagen County.

N/TERT-1 immortalized human keratinocytes (male) and N/TERT-1 hRas[56] were kindly provided by James G. Rheinwalds lab, Harvard Institute of Medicine, Brigham & Womens Hospital. Cells were maintained in K-SFM (Gibco) supplemented with 25 μg/ml BPE (Gibco), 0.2 ng/ml EGF (Thermo Scientific), and 0.3 mmol/l $CaCl_2$ (Sigma) at 37°C with 5% CO_2 as previously described.[55] N/TERT-1 p53 KO was made in previous studies.[26,55]

Organotypic cultures were prepared as described previously.[26,28,57] Briefly, human fibroblasts were suspended in Type I collagen (4 mg/ml) and allowed to polymerize in six-well culture inserts with 3-μm-pore polycarbonate filters (BD Biosciences NJ, USA). Gels were allowed to contract for 4–5 days before seeding with $3x10^5$ N/TERT-1 keratinocytes in DMEM/F12 raft medium supplemented with 1.5% FCS (HyClone), 5 μg/ml insulin (Sigma Aldrich), 0.1 nM choleratoxin (Sigma), 400 ng/ml hydrocortisone (Sigma), 0.02 nM triiodothyronine, and 0.18 mM adenine (Sigma). Inserts were raised to the air-liquid interface 4 days after cell seeding and cultured for additional 10 days. Organotypic cultures were fixed in PFA prior to sectioning.

METHOD DETAILS

Differentiation of macrophages and moDCs

Monocytes were generated from isolated PBMCs from blood donor buffy coats. For all studies, monocytes were purified within 24 h of the blood being drawn. The PBMCs were separated by gradient density centrifugation using Lymphoprep (Stem Cell Technologies) and $5x10^6$ cells/mL plated in 6-well plates (Corning, Primaria coated) in RPMI 1640 with Glutamax (Gibco) containing 15% heat-inactivated human AB serum (Sigma-Aldrich). After adhesion for 80 min at 37°C in a humidified incubator, plates were shaken to release unbound cells. The wells were then washed 3-4 times in RPMI 1640. Finally, RPMI 1640 with Glutamax and 5% heat-inactivated human AB serum was added. The media was further supplemented with 100 ng/mL human recombinant GM-CSF, 100 ng/mL M-CSF (Peprotech), or 50 ng/mL human recombinant GM-CSF and 25 ng/mL human recombinant IL-4 for APC differentiation into M1-like MΦs, M2-like MΦs, and DCs, respectively. Cells were cultured for 6 days and the media and cytokines refreshed on day 3. On day 5, M1-like MΦs, M2-like MΦs, and DCs were stimulated with recombinant human Gal-1 (300 ng/mL, 24 h). On day 6, samples were harvested by removing the media and washing the cells with PBS one, after 0.5% BSA, 2mM EDTA in PBS was added and incubated 30minutes at 4°C to let the cells detach. Then the cells were scraped with a cell scraper and pooled with the earlier harvested media and the cells and supernatant were centrifugated for 5 minute at 300g. The cells were washed with PBS and further processed for RNA sequencing. RNA sequencing was performed by BGI Headquarters (China).

Production and fluorescent labeling of galectins

The oxidation-stable Gal-1 C3S mutant was produced in *E. coli* BL21 Star (DE3) cells (Invitrogen) and purified by affinity chromatography on lactosyl-Sepharose as described previously.[54] Purified Gal-1 was lyophilized and stored at -20°C until use. Protein concentrations were measured using BCA assay (Thermo Fisher Scientific) and spectrophotometric data analyzed in Graphpad Prism software. For cell surface binding experiments, galectins were fluorescently labeled using NHS-fluorescein (Thermo Fisher Scientific). Briefly, the dye was dissolved in DMSO and added at a 10-fold molar excess to 2 mg/mL galectin solution in coupling buffer (20 mM HEPES). The solution was kept in the dark and incubated at room temperature with continuous mixing for 1 h. Labeled galectins were separated from unreacted dye by buffer exchange with PBS on a PD10 column (GE Healthcare).

Galectin cell surface binding

Monocyte-derived M1-like MΦs, M2-like MΦs, and DCs were generated as described above. Cells were harvested by scraping in cold PBS followed by a wash with 5 mL of PBS containing 100 mM lactose (Sigma) to remove bound endogenous galectins. This was followed by an additional wash in 5 mL of PBS to remove excess lactose. A cell viability of >90% was confirmed using a trypan blue staining. Measurement of galectin surface binding was then performed as described previously.[9] Final galectin concentrations were 0-4800 ng/mL, and propidium iodide (PI) was added to a final concentration of 50 μg/mL immediately prior to data acquisition. Flow cytometry was performed using an LSRII cytometer (BD Biosciences) and data analyzed using FlowJo software. Single cells were selected using a FSC-A x FSC-H gate and permeable (PI positive) cells were excluded from analysis. Fluorescence data were collected using logarithmic amplification on 30,000 light scatter-gated events (cell counts). Data points for binding curves were calculated as GMFI values for cells treated with galectin, subtracted by GMFI values for lactose inhibition controls.

Proteomics data acquisition by mass spectrometry

To achieve increased number and purity as required for proper acquisition and analysis, monocytes were isolated using CD14 magnetic beads (Miltenyi) according to manufacturer's protocol, from four individual donors. On day 6, M2-like MΦs were stimulated with or without galectin-1 (300 ng/mL) for 0 min, 5 min, 6 h, or 12 h. Cells were then washed twice with cold PBS and then rapidly lysed, reducing and alkylating cysteines in a single step. Briefly, boiled 2% sodium dodecyl sulfate (SDS) in 50 mM tris(2-carboxyethyl)phosphine (pH 8.5) was added directly to the cells. Lysis buffer containing cells was boiled for an additional 10 min at 99°C, followed by sonication for 2 min. Cell digestion was performed with an automated protein aggregation capture (PAC) pipeline as described previously. PAC digestion was performed on a KingFisher™ Flex robot (Thermo Fisher Scientific) in a 96-well plate.

For cells from Donor 1, digested samples were purified on SepPak (C18 Classic Cartridge, Waters, Milford, MA) and 120 μg of peptides from each sample were labeled by TMTpro 16plex reagents (Thermo Fisher Scientific). Labeled samples were then pooled and purified again on SepPak cartridges. We reserved 10 μg of pooled peptides for proteome samples and used the rest for phosphopeptide enrichment with Ti-IMAC beads (ReSyn Biosciences) on the KingFisher™ Flex robot as described previously. The reserved peptides and enriched phosphopeptides were then subjected to offline high pH reverse phase fractionation. We collected 46 and 24 fractions for peptide and phosphopeptides samples, respectively. The eluate was dried using a SpeedVac, re-dissolved in 0.1% FA, and then loaded on EvoTips. For cells from Donors 2, 3, and 4, digested samples were purified on SepPak (C18 Classic Cartridge, Waters, Milford, MA) and then 500 μg of peptides from each sample with at least two technical replicates were loaded on EvoSeps. All samples were analyzed on an Orbitrap Exploris 480 mass spectrometer coupled with an Evosep One system using an in-house packed 15 cm, 150 μm i.d. capillary column with 1.9 μm Reprosil-Pur C18 beads (Dr. Maisch, Ammerbuch, Germany) and the pre-programmed gradients (30 samples per day). For TMTpro samples, full MS resolution was set to 60,000 at m/z 200 with the AGC target at 300%. MS2 resolution was 45,000 for proteome samples and 30,000 for phosphoproteome samples. The normalized collision energy for HCD was set to 32%. Samples from Donors 2, 3, and 4 were analyzed in data-independent acquisition (DIA) mode as described previously.

Proteomic data processing

All DDA raw files were processed in Proteome Discoverer 2.4 (Thermo Fisher Scientific) with the human SwissProt FASTA database (20,355 entries, March 2019). Trypsin was set as the digest enzyme and up to two missed cleavages were allowed. TMTpro was specified as a fixed modification on lysine and the peptide N-terminus, and methionine oxidation was specified as a variable modification. In addition, phosphorylation was set as a variable modification on serine, threonine, and tyrosine residues in phosphoproteome samples. All raw DIA files were processed with Spectronaut (Biognosys, Zurich, Switzerland) in DirectDIA mode. Default settings were used in Spectronaut for peptide identification and quantification. Statistical analysis and functional enrichment were conducted with R scripts written in-house mainly using clusterProfiler and DAPAR packages. Mfuzz[21] package was used for the soft clustering with default settings.

Western blot

Whole cell lysates were prepared, and protein concentration measured by standard BCA assay. Equal amounts of protein were separated on a 4-12% BisTris SDS-PAGE gel and transferred to a 0.2 mm-pore

nitrocellulose membrane. For detection of IDO1 protein, western blotting was performed using a WesternBreeze® kit according to the instructions provided by the manufacturer (WB7104, Thermo Scientific). For detection of all other proteins, membranes were washed briefly in MQ, blocked in 5% BSA for 30 min at room temperature before being incubated with primary antibody in 5% BSA overnight at 4°C. The next day, membranes were washed three times for 5 min in TBS-T and then incubated with HRP-conjugated secondary antibody for 1 h at room temperature. Membranes were washed three times for 5 min, developed using SuperSignal™ (Thermo Scientific™), and imaged by ImageQuant LAS 4000 (GE Healthcare Lifesciences). The following primary antibodies were diluted in 5% skimmed milk in TBS-T or 2.5% BSA in TBS-T as required: anti-IDO1, clone 1F8.2 (1:1000, Cat. MAB10009, Sigma-Aldrich), anti-α-tubulin (1:2000, Cat. ab4074, Abcam), anti-phospho-STAT3 (Y705) antibody (Cell signaling Technologies D3A7 XP, Rabbit mAb #9145) and anti-GAPDH antibody (Abcam, #ab8245). Secondary antibody was HRP-conjugated mouse-anti rabbit (1:4000, Dako/Agilent).

Kynurenine kinetic assay

M1 and M2-like MΦs were stimulated with 300 ng/mL or 600 ng/mL Gal-1 ± lactose (100 mM) and incubated 24 h at 37°C. Then 100 μM L-Trp (Merck) was added after 2 h of incubation. 120 μL of the culture media was harvested, mixed it with 30% trichloroacetic acid (Sigma-Aldrich), and incubated for 30 min at 50°C. Precipitates were separated by 10 min centrifugation at 2270 x g. A total of 75 μL of the supernatant was mixed with an equal volume of freshly prepared 2% Ehrlich reagent (4-(dimethylamino)-benzaldehyde, Sigma Aldrich) and incubated for 15 min at room temperature in the dark. Absorbance was measured at 492 nm. Different concentrations of kynurenine acid were used as a standard.

Immunofluorescent tissue staining

FFPE tissue sections were de-paraffinized and rehydrated, followed by heat-induced epitope retrieval. Sections were then fixed in 4% PFA for 10 min at room temperature, washed in PBS for 5 min, permeabilized in 0.3% Triton X-100 for 3 min, then washed twice in PBS for 5 min before incubation with primary antibodies at 4°C overnight. The next day, sections were washed three times in PBS and mounted with ProLong Gold Antifade with DAPI (Thermo Fisher). For Gal-3 staining, frozen tissue sections were air-dried, incubated for 5 min in ice cold methanol/acetone (1:1), and incubated with primary antibody at 4°C overnight, then processed as FFPE tissue sections from hereon. The following primary antibodies were used: anti-galectin-1 (1:500, ab25138, Abcam), anti-galectin-3 (1:500, MAB11541, R&D), anti-galectin-8 (1:200, ab109519, Abcam), and anti-cytokeratin 10 (K10) (1:100, M7002, Dako (Agilent). The following secondary antibodies were used: goat anti-mouse Alexa Flour 594™, goat anti-rabbit Alexa Flour 488™, and goat anti-mouse Alexa Flour 488™. Confocal images were acquired with LSM 780 AxioObserver (Zeiss) with a 20x objective. Quantification was performed using Zen software, based on a trained intellesis segmentation model. Data is presented as the fold change of the average of triplicates.

qPCR

Total RNA was collected from unstimulated and Gal-1-stimulated M1-like MΦs, M2-like MΦs, and DCs and treated with DNase I. The RNA concentration was determined on NanoDrop. RNA was reverse-transcribed to cDNA and qPCR performed. mRNA encoding IDO1 was quantified using a specific pre-designed fluorescent probe. All experiments were performed in triplicate, and mRNA encoding IDO1 and GAPDH expression were quantified. Relative gene expression levels were expressed as the fold change relative to untreated samples.

Gene symbol	Assay ID	RefSeq transcript	Exon boundary	Amplicon length
IDO1	Hs00984148_m1	NM_002164.5	6 - 7	66
GAPDH	Hs02758991_g1	NM_001256799.1 NM_002046.4	6 - 7	93

MS-based glycan profiles

N-linked glycans were profiled on monocyte-derived M1-like MΦs, M2-like MΦs and DCs dissolved in 0.1% Rapigest (Waters) and incubated on ice while vortexing every 5 minutes. Samples were then centrifuged at

10,000 x g for 10 min and the supernatant collected and reduced with 5 mM DTT (Sigma) for 1 h at 60°C, followed by alkylation with iodoacetamide (Sigma) for 30 minutes at room temperature in the dark. Samples were digested with 5 μg trypsin (Roche Diagnostics) overnight at 37°C and peptides purified using a Sep-Pak 1-cc C18 cartridge (Waters). Organic solvent was removed by SpeedVac and pH adjusted to 7-8 with 50 mM ammonium bicarbonate, followed by overnight digestion with 3 U PNGase F (Roche diagnostics) at 37°C. Released N-glycans were cleaned up using a Sep-Pak 1-cc C18 cartridge and lyophilized. For N-glycan profiles, dried samples were permethylated as described previously[58] and analyzed by positive reflector mode MALDI-TOF (AutoFlex Speed, Bruker Daltonics) with data acquisition in the 1000-7000 m/z range.

Flow cytometry

An equal number of each cell type was analyzed for each assay. Cell viability was evaluated before the staining with the different antibodies by trypan blue stain, applying a viability requirement of > 80 % for cells to be included for analysis. Monocyte-derived M1-like MΦs, M2-like MΦs and DCs were blocked in ice-cold PBS with 2% human AB serum and incubated with primary antibody, diluted in ice-cold PBS with 2% human AB, for 30 min on ice. Following, cells were centrifuged and washed 3 times in ice-cold PBS with 2% human AB, before incubation with secondary antibody as required. Lastly, cells were 3 times in ice-cold PBS with 2% human AB and finally resuspended in 100μL ice-cold PBS with 2% human AB for analysis. The following primary antibodies were used; anti-CD206 (Biologend, clone 15.02), CD11c-PE (BD Pharmingen ref 555392), anti-CD14-PE (Dako clone TÜK4), CD163-APC (Biolegend ref 333609), anti-HLA-DR/DP/DQ-FITC (MHC Class II-FITC) (Dako clone CR3/43), CD80-FITC (Dako), anti-CD40-APC (Biolegend), anti-CD86-PE (Dako). Secondary antibody Alexa Fluor 488 goat anti-mouse IgG (H+L). Isotype controls, mouse IgG-FITC, PE, APC (all BD Pharmingen). Secondary background staining or isotype controls were determined for all individual samples. To clarify the gating strategy for Figure 2B, we showed a representative figure (Figure S7) demonstrating the gating strategy applied to M1-like MΦs, M2-like MΦs and DCs. The top panel shows gating of the population analyzed based on FSC-A/FSC-H scatter plots. The second panel shows gating of singlets based on SSC-A/SSC-H plots. The last panel shows analysis of the singlet population, for the indicated markers, here shown for the lineage-specific marker CD206 for M1-like MΦs and DCs and CD163 for M2-like MΦs. Analysis of non-stained and isotope controls were included for all cell types and all markers. Samples were run on a BD Fortessa3 and SONY Spectral Cell Analyzer (SONY SA3800) flow cytometer and analyzed by FlowLogic software and FlowJo v10. The Flow analysis was performed on a total minimum of 10 000 events. Exclusion of cell debris was conducted by SSC-A and FSC-H gating and doublets were based on FSC-A/FSC-H plot to ensure analysis based on singlets.

Immunofluorescent cell staining of APCs

To investigate the cell morphology of polarized M1-like MΦs, M2-like MΦs and DCs, cells were seeded on poly-L-lysine-treated coverslips ($5x10^4$ cells in RPMI 1640) for 18 h (37°C, 5% CO_2) for 2 or 5 days of polarization, after which cells were fixed in 4% (v/v) paraformaldehyde in PBS followed by permeabilization with 0.03% Triton x-100. Subsequently, cells were blocked in 2.5% BSA in PBS and stained against F-actin by labeling the cells with phalloidin 1:250 in 2.5% BSA. Lastly, cells were mounted with ProLong Gold mounting medium with DAPI. Images were captured using the Leica Microsystems Fluorescence Microscope (20x magnification).

QUANTIFICATION AND STATISTICAL ANALYSIS

Statistical analyses of the survival analysis in head and neck cancer and pancreatic cancer was done at GEPIA with default settings (http://gepia2.cancer-pku.cn). Statistical analysis and functional enrichment for the generated proteomic data are described in detail in the above "proteomic data processing" section. Flow cytometry plots were generated in flowjo V10 and statistical data analysis was performed in flowjo V10 and GraphPad Prims V8. Sample number (n), replicates and statistical method used are described in each figure legend.